A comparison of coupled and de-coupled simulation procedures for the fatigue analysis of WEC mooring lines

Shun-Han Yang[1*], Jonas W. Ringsberg[1], Erland Johnson[1,2], ZhiQiang Hu[3] and Johannes Palm[1]

[1] Chalmers University of Technology, Department of Shipping and Marine Technology, Division of Marine Technology, SE-412 96 Gothenburg, Sweden
[2] SP Technical Research Institute of Sweden, Department of Structural and Solid Mechanics, P.O. Box 857, SE-501 15 Borås, Sweden
[3] Shanghai Jiao Tong University, State Key Laboratory of Ocean Engineering, Shanghai, 200240, China

* Corresponding author: (e-mail) Shunhan.Yang@chalmers.se; (phone) +46-(0)31-7726067

Abstract
Mooring systems for floating wave energy converters (WECs) must be designed to survive the cyclical loads and motions to which they are subjected as a result of the wave load-WEC interaction and the motions of the WEC in the random elevation of the sea surface. The current study compares simulation procedures for the fatigue analysis of WEC moorings. The objective is to suggest a simulation procedure suitable for an extensive study of the behaviour of WEC systems and thus for the fatigue analysis of mooring lines. A cylindrical, floating WEC with four spread mooring lines is chosen as case study. The dynamics of the WEC system are simulated and analysed using both coupled and de-coupled models in the time-domain. Four types of simulation procedures are compared using commercial software, DNV DeepC, and an in-house solver, MooDy. A systematic fatigue response analysis based on variations of the numerical and physical parameters is conducted. The results are compared with respect to the fatigue damage calculated using the stress-based approach and the rainflow counting method. The simulation procedure using a coupled model is suggested as the preferred numerical method for capturing the interaction between the components of WEC system, which is proven to be crucial for the fatigue damage evaluation of mooring lines.

Keywords: coupled model, de-coupled model, fatigue, mooring line, wave energy converter

1 Introduction
The oceans are full of waves which could greatly contribute to supply the world with emission-free energy. Hence, exploiting the ocean wave energy as a sustainable source of renewable energy has gained increasing attention worldwide. Barstow et al. (2008) presented a map of the global annual mean wave power estimates in order to highlight the areas where the wave energy resource has its largest development potential: the highest energy level in the Northern Hemisphere are off the west coast of the British Isles, Iceland, and Greenland, while the highest energy level in the Southern Hemisphere are located off Southern Chile, South Africa, and the south and south west coasts of Australia and New Zealand. Jacobsen (2011) presented an example showing that the recoverable wave energy along the coastlines of the United States is in the order of 1000 TWh/year. This corresponds approximately to 1/3 of the total electricity consumption of the United States. In Europe, the wave resource is anticipated to be 29500 TWh/year (Magagna et al. 2014). The UK's Carbon Trust estimated that the global wave and tidal energy market could be worth up to € 535 billion between 2010 and 2050 (Carbon Trust, 2013).

Advancements in several research areas for wave energy converters (WECs), such as numerical simulations, experimental studies, power take-off systems, control strategy, and novel material in different components, have increased both their attractiveness and their

economic viability, see ISSC 2015 committee V.4 (Gao et al., 2015). In this reference, different wave energy conversion technologies used to harvest the energy are categorised based on their fundamental functioning principle: oscillating water column, oscillating bodies, and overtopping. It becomes evident that the technology chosen should match the specific site conditions in order to strive for economic viability (Barbarit et al., 2012; Falcão, 2010). However, an additional complexity regarding the limitation of long-term operation of WEC systems and their commercial impact is the mechanical service life (Ambühl et al., 2015; Thies et al., 2011a). This issue is addressed in the current investigation which focuses on the established state of initial design of mooring lines with respect to their long-term usage, *i.e.*, fatigue limit state design. The research is motivated by examples presented in the literature which highlight that mooring lines are considered to be a critical component in the long-term usage of WECs (Fitzgerald, 2009; Johanning et al. 2006; Martinelli et al. 2012).

The focus of research and development of WECs and their components shifts from single device solutions to WECs installed in arrays (Babarit, 2013; Gao et al., 2015). Siddorn and Taylor (2008) and Vicente et al. (2009a) showed that if point absorber WECs are employed in the extensive exploitation of the offshore wave energy resource, they should be deployed in the form of arrays. A question that arises in this context is whether the fatigue design of a mooring line can be treated as a single component for a stand-alone WEC, or, if it has to be considered as a component in a larger array of WECs. Additionally, which simulation procedure should then be used to carry out this initial fatigue design? Several references in the literature present investigations where, among others, power capture, motion behaviour of WECs, and mechanical characteristics of moorings are studied using the de-coupled simulation procedure; see for instance Fitzgerald and Bergdahl (2008), Harnois et al. (2015), Liu and Bergdahl (1997), Vicente (2009b), Vicente et al. (2011a), and Vicente et al. (2011b). There are also several investigations on the same topics where the coupled simulation procedure is used, see for instance Bhinder et al. (2015), Cerveira et al. (2013), and Palm et al. (2013). But, there is a gap of investigations in the public literature providing clear recommendations about which simulation procedure that should be used in the initial fatigue design of mooring lines.

1.1 Mooring, fatigue and objective of the study

One of the key engineering issues of the design and installation of floating WECs is to make sufficiently accurate predictions regarding the maintenance, durability, and reliability of the mooring systems, the marine power cables, and the load-bearing components (Thies et al., 2011a; Thies et al., 2011b; Thies et al., 2012; Thies et al., 2014a; Thies et al., 2014b). Traditionally, the wave energy market has employed mooring concepts adopted from the technology in the oil and gas industry, where chains or wire mooring are often used (Gao et al., 2015; Johanning et al., 2006; Thomsen et al., 2015). For mooring systems used in WECs, where highly compliant behaviour is needed, Ridge et al. (2010) investigated the option of using nylon fibre rope moorings. However, many mooring system designs and analyses are still conducted on moorings made of metallic materials (Abouelfadl et al., 2013; Christiansen et al., 2013; López-Pavón et al., 2013; Murphy et al., 2015; Soulard et al., 2013).

In the design and assessment of mooring systems, simulation procedures often referred to as de-coupled and coupled models can be used; see Sections 2 for details. In the de-coupled model used in the current study, the motions of a WEC are calculated first, independently and without influence from its mooring system. The motion of each mooring line is thereafter calculated using the already calculated motions of the WEC as prescribed boundary conditions in the fairlead points (*i.e.* the connection points between the WEC and its mooring lines). This simulation procedure reduces the complexity of the numerical simulation and often offers better numerical stability compared to the coupled model. In this model, the

motion of the WEC and its mooring lines are solved simultaneously. The merit lies in the inclusion of mutual interaction (coupling) effects between the WEC and the mooring lines in the simulation (such as inertia load and damping effect from the moorings, and seabed friction).

Both simulation procedures have been applied extensively for various purposes. The de-coupled model has been used by among others Fitzgerald and Bergdahl (2008) who investigated the effect of mooring layout on the motion and power performance of a generic WEC; Vicente et al. (2009b) compared the difference in energy absorption between an unmoored and an independently moored WEC, where the WEC is put in an triangular three-buoy array configuration; Harnois et al. (2015) described the detailed validation of a numerical de-coupled model of wave energy mooring system using tank test result. The presented numerical model and methodology can further be used by wave energy developers in the development of cost-effective mooring systems which will contribute to the efficiency of wave energy devices. As a comparison to the de-coupled simulation procedure Cerveria et al. (2013) used a coupled model and concluded that a catenary chain mooring system has negligible influence on the floating wave energy dynamics and captured wave energy. Palm et al. (2013) developed a coupled model that is capable of capturing the effects of breaking waves, loads under green water conditions on the WEC as well as nonlinear mooring forces and snap loads, all of which are crucial for correct estimates of the extreme loads acting on the system in violent seas. Bhinder et al. (2015) applied the coupled simulation procedure in a comparison of three commercial software packages, ANSYS AQWA, OrcaFlex and SIMA, and studied the nonlinear and temporal behaviour of synthetic ropes, geometric mooring line nonlinearities, and nonlinear viscous fluid damping. Numerical simulations were carried out on the same WEC system. A comparison of the results from the WEC's motions from the different simulation codes agreed in general, while the estimated mooring line forces showed less agreement.

In the initial design phase of a WEC system, the level of accuracy and physics incorporated in the simulation model must be adjusted depending on the purpose of the analysis *e.g.* motions of the buoy, power capture, or structural response (fatigue) of the moorings (Davies, 2009; DNV, 2005). The current investigation addresses the long-term usage and safety of the mooring lines. The intention is to compare the coupled and the de-coupled simulation procedures and discuss their suitability in the initial fatigue design assessment of WEC mooring lines before the detailed design is carried out. It is well-known that both prototype and full-scale field measurements provide important input data and allow models to be validated, but these measurements are too scarce and costly to present a stand-alone alternative at the time of writing (Harnois et al., 2015; Johanning et al., 2007; Paredes, et al. 2015). Hence, numerical simulation procedures have an important task to accomplish especially in the initial design phase, *i.e.* which simulation procedure that should be adopted to make "reliable" fatigue life assessment. This chosen procedure will also be crucial for the subsequent detailed analysis of mooring systems and their configurations.

The study and comparison of simulation procedures focus on the analysis of one WEC and its moorings, namely one buoy among several buoys in an array. This system is considered as an essential subsystem of an array of WECs and their moorings, and it enables a detailed comparison of the pros and cons between simulation procedures. The main objective is therefore to compare the different simulation procedures, leading to a recommendation for initial fatigue design assessment of WEC mooring lines. The study is purely numerical, but, it includes a fatigue response analysis which shows how numerical and physical parameters, and the choice of simulation procedure, influence the results. This contributes to better understanding and knowledge how the studied WEC system reacts on parameter changes and

choice of simulation procedure. In addition, it is discussed how motions, forces, and stress responses of the mooring lines vary between the simulation procedures.

A schematic layout of the case study "WEC system" model is presented in Figure 1. This model consists of the WEC, the mooring lines, and the environmental conditions, all of which governing the operating conditions, production of energy, and reliability (service life) of the mooring system. The environmental conditions in Figure 1 are composed of seawater, wave and seabed; the influence from wind and current is disregarded in this study. Each mooring line is connected to the WEC and to the seabed by a fairlead and anchor, respectively.

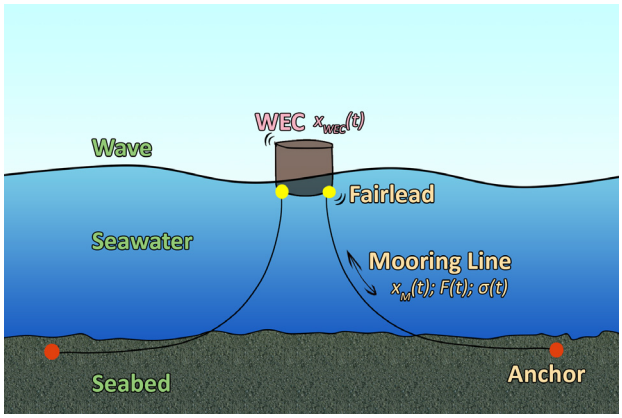

Figure 1 Schematic layout of a WEC system and its components; see Section 3 for details.

The outline of this study is as follows: Section 2 presents the methodologies that are used and compared in the current study. Section 3 presents the WEC system, its theoretical basis and the case study model. Section 4 presents the results from the reference case in Section 3, followed by a systematic fatigue response analysis and discussion in Section 5. An example of a fatigue damage analysis under irregular wave conditions is presented in Section 6. The conclusions from the study are finally presented in Section 7.

2 Methodology

A reliable fatigue analysis of WEC mooring lines requires that the entire system be analysed. This analysis is necessary because the accuracy in the fatigue life prediction is both sensitive to and affected by variations in both the physical properties and the numerical parameters of the model. For example, the coupling between environmental conditions, motions of the WEC and motions of the mooring lines each influence the accuracy of the calculated values of the stresses and the fatigue assessment of mooring line.

The study presents a systematic analysis of a WEC system with a cylindrical floating WEC and four spread mooring lines. It is divided into the following major steps; see Section 3 for details and Figure 2 for a workflow of the simulation procedures:

- **Definition of physical characteristics:** the physical properties for the WEC system including the WEC, the mooring system, seabed, seawater and waves.
- **Definition of numerical setting:** the numerical parameters used in the numerical simulation.
- **Hydrodynamic analysis:** the simulation and analysis of the motion behaviour of the WEC, $\boldsymbol{x}_{WEC}(t)$, and the mooring lines, $\boldsymbol{x}_M(t)$.
- **Structural analysis:** the calculation of the force response in the mooring lines, $\boldsymbol{F}(t)$.
- **Stress response analysis:** the calculation of the mooring line stress matrix, $\sigma(t)$.
- **Fatigue damage analysis:** the calculation of the fatigue damage and lifetime prediction based on the mooring line stresses.

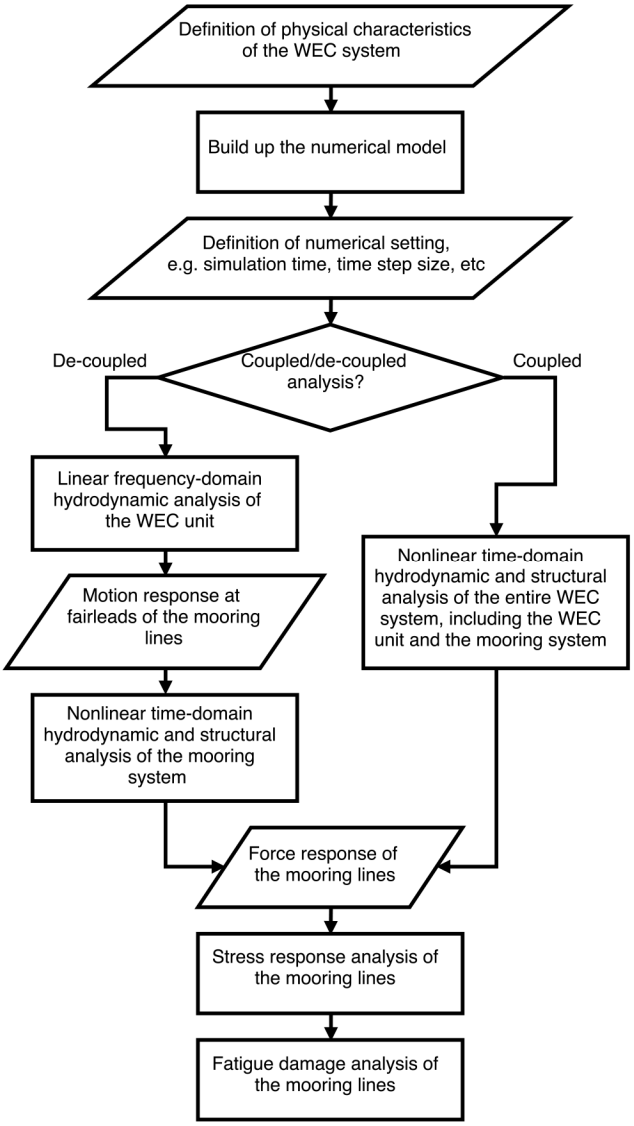

Figure 2 Workflow of the simulation procedures used in the current study.

The dynamics of the WEC are simulated and analysed using both coupled and de-coupled models. In the de-coupled model (the left track in Figure 2), a simulation is carried out in two subsequential steps. First, the motion responses of the WEC are calculated in a linear frequency-domain analysis. The motion responses at the fairleads of the mooring lines are post-processed and transferred to the time-domain. Secondly, in the following nonlinear time-domain simulations, the responses in the mooring lines are calculated based on the previously calculated motion responses in the fairleads as prescribed boundary conditions. Due to the obvious lack of coupling between the mooring lines' influence on the WEC's motions, this technique has the following shortcomings due to the separated steps:

- The damping effects from the mooring system on the low-frequency motion can only be included by additional approximation.
- The dynamics of the mooring lines are not influential to the wave frequency motion of the WEC.

- The seabed friction and frictional forces due to the WEC/mooring lines contact are excluded in the de-coupled model.

In the coupled model (the right track in Figure 2), the equations of motion of both the WEC and its mooring lines are simultaneously solved using a nonlinear time-domain analysis. As a result, the motion of the mooring lines implicitly influences the instantaneous mean position and dynamic response of the WEC. More accurate predictions are expected by using the coupled model and taking the following effects into account:

- The seabed friction, which affects the dynamics of the mooring lines and the WEC.
- The damping and friction due to the viscous force acting on the mooring lines.
- The static restoring force from the mooring lines as a function of the motion response of the WEC, which changes the mean position and dynamic response of the WEC.
- The inertia loads due to the mooring system and the hydrodynamic loads acting on the mooring lines.

Numbers of software programs, such as OrcaFlex (STA, 2014), WEC-Sim (NREL and SNL, 2014) and DeepC (DNV, 2013a), can be used for the hydrodynamic and structural analyses of WECs and their moorings. However, there is no consistent evidence that shows which software program and which simulation procedure are most suitable for the fatigue analysis of mooring lines. In this investigation, DeepC is chosen due to its integrated function to simulate an entire deep water floating system in which the WEC, mooring system and environment conditions are all modelled and evaluated in one toolbox. An in-house solver, MooDy (Palm, 2014), is also used to compare the motion and the structural analysis of the mooring lines.

DeepC is a software that incorporates a number of solvers that can be used to simulate and analyse deep water floating marine structures (DNV, 2004). Since 1996, the main simulation features of DeepC have been extensively verified and validated by numerous researches (DNV, 2004). In this study, SIMO (MARINTEK, 2012a) is used to simulate the motion behaviour of the WEC and RIFLEX (DNV, 2013b) is used to perform the motion analysis and structural response simulation of the mooring lines.

MooDy is an in-house finite element (FE) solver developed for the analysis of mooring lines and cables. It has been verified and validated by Palm (2014) and has previously been used to analyse a similar WEC system (Palm et al., 2013). Through an automated program interface, MooDy can be used for coupled simulation procedure by interacting with an external solver for the hydrodynamic analysis of the WEC. In this study, however, it is used as a stand-alone mooring solver with a prescribed motion time history at the fairleads.

Table 1 presents an overview of the four types of simulation procedures that are completed and compared in this study. T1 and T3 are both carried out by DeepC, but they differ in terms of the simulation procedures. T1 uses a de-coupled model in which the motions of the WEC are solved in the frequency-domain to obtain the response amplitude operator (RAO) of the buoy, and then the mooring system's response is solved in the time-domain. The two separate and sequential steps are referred to as DeepC-RAO and DeepC-RIFLEX, respectively. T3 uses a coupled model in which the entire system is solved in the time-domain. This simulation for the WEC is referred to as DeepC-Time, and simulation for the mooring system is referred to as DeepC-RIFLEX. Interactions occur between DeepC-Time and DeepC-RIFLEX at every time step throughout the entire simulation.

T2 and T4 are both carried out by MooDy to compare the simulation results from MooDy with the DeepC (DeepC-RIFLEX) results. To perform the mooring analysis, the motion response at the fairleads computed by T1 and T3 is used as input data for T2 and T4,

respectively, being the excitation for the mooring system. Both of T2 and T4 are defined as de-coupled analyses.

Table 1 Presentation of the four types of simulation procedures that are compared in the current investigation.

Types	Analysis	Motion analysis of the WEC $\boldsymbol{x}_{WEC}(t)$	Motion and structural analysis of the mooring lines $\boldsymbol{x}_M(t);\ \boldsymbol{F}(t);\ \sigma(t)$
T1	De-coupled	DeepC-RAO	DeepC-RIFLEX
T2	De-coupled	Motion at the fairleads from T1	MooDy
T3	Coupled	DeepC-Time	DeepC-RIFLEX
T4	De-coupled	Motion at the fairleads from T3	MooDy

3 Model of the wave energy converter system

The WEC system and its different components were introduced in connection with Figure 1. The physical and numerical models of these components will now be elaborated. Figure 3 presents the initial configuration of the system components together with a Cartesian coordinate system. The WEC is floating on the surface in a water volume with infinite extent in the horizontal *x*- and *y*-directions. It has a finite depth, denoted by *h*, and the depth direction is in the negative *z*-direction. To enable systematic and detailed comparisons of T1 to T4, the WEC is exposed to regular waves propagating in the positive *x*-direction and at the same time connected to four mooring lines along the *x*- and *y*-directions, as shown in Figure 3. Each one of the four mooring lines is attached to the underlying seabed but the WEC is free to move with the waves. In the following sections, the models of the different system parts, namely the wave water volume, WEC, mooring system, and seabed, and the numerical simulation method will be further explained.

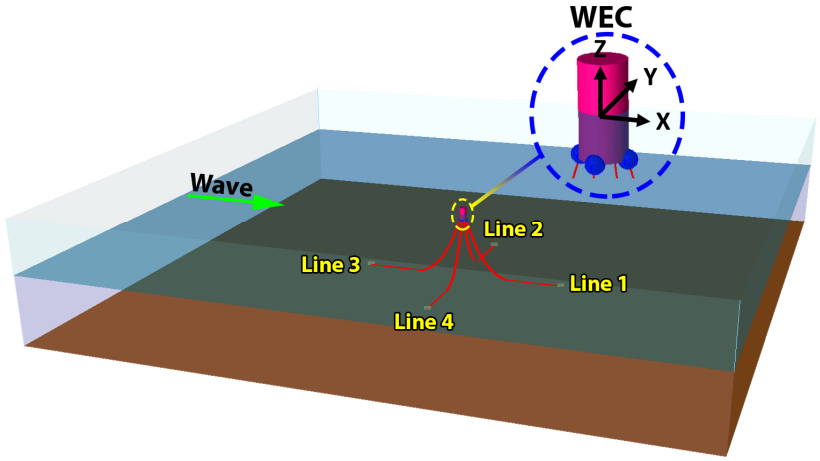

Figure 3 Illustration of the set-up of the WEC system comprised of the WEC, the four mooring lines, the water with waves, and the seabed. A Cartesian coordinate system, *xyz*, defines the orientation of the illustration, where the origin is located at the water surface at the WEC equilibrium position.

3.1 Water and wave loading

The environmental parameters from the water and waves are summarised in Table 2. The water is modelled as incompressible, inviscid and irrotational fluid. Thus, the theory is based on the potential flow with the velocity components uniquely determined by the gradient of a harmonic velocity potential. Furthermore, restrictions are made under the assumption of small

wave amplitude and to follow Airy theory (DNV, 2012; MARINTEK, 2012b). Although the water is assumed to be inviscid, a nonzero kinematic viscosity has been introduced to model the viscous drag effect of the water on the mooring lines yet pose no effect on the WEC motion.

The boundary conditions consist of both kinematic and dynamic conditions. A kinematic condition states that a fluid particle on the water surface will stay on the free surface, and a dynamic condition states that the water pressure on the surface is equal to the atmospheric pressure on the free surface. Under Airy theory, the mean free surface, defined as still water level z=0, must satisfy both boundary conditions mentioned above. At the seabed, which is assumed to be horizontal and at a depth of z=-h, the condition is zero normal velocity, whereas the tangential velocity is unspecified.

Table 2 Environmental conditions in the case study.

Water	
Acceleration of gravity, g [m/s^2]	9.81
Density, ρ [kg/m^3]	1,025
Kinematic viscosity, μ [m^2/s] (only for viscous drag effect)	$1.19 \cdot 10^{-6}$
Still water mean level, Z [m]	0
Water depth, h [m]	50
Wave	
Wave direction [degrees]*	180
Regular wave height, H_w [m]	2
Regular wave period, T_w [s]	7

* The angle is measured (positive) clockwise from the x-axis.

The WEC system in the study is only subjected to loads from waves, *i.e.* currents and wind loading are not considered. A floating WEC is typically designed to be in resonance with the encountered wave to maximise the extraction of the wave energy (Berteaux, 1976; Budar and Flanes, 1975). The resonance condition for the current WEC configuration corresponds to a wave period of 5 s. Since the linearization, introduced by Airy theory and the de-coupled model (see Section 3.2) sets an upper bound on the steepness of the wave and the amplitude of the body motion, see MARINTEK (2012b) for details, a wave with period T_w=7 s at a wave height of H_w=2 m was chosen for the study. Being slightly above resonance, this selection enables reliable comparisons of fatigue damage in each mooring line for the different simulation procedures (Fitzgerald and Bergdahl, 2008).

3.2 Wave energy converter

In this study, a cylindrical buoy represents a floating point absorber type of wave energy converter (FPA WEC). Although it is subjected to strong heave and pitch motions, this type of WEC exploits more powerful wave regimes available in water depths typically more than 40 m (Falcão, 2010). The WEC is modelled with the geometry, mass, and damping parameters shown in Table 3 and floats on the water surface, z=0. The geometric centre of the cylinder intersects with the free water surface at still water conditions. Hence, the origin of the global coordinate system is defined in this point (see Figure 3). The mass of the cylinder is concentrated to its mantle surface and bottom plate. This concentration is used to ensure that the buoy will remain in stable equilibrium with a positive metacentric height at static condition. Finally, an additional damping, D_{PTO}, with six degrees of freedom (DOFs) is introduced to incorporate the linear power take-off (PTO) damping for power production in

the model. An idealised linear PTO damping set-up is used based on the Fitzgerald and Bergdahl (2008) model where the dampers are somehow connected to earth.

The incident wave field described above is disturbed by the WEC through radiation and diffraction effects. Similar to the incident wave field, the effects of radiation and diffraction are described by separate potential fields. Because linear theory is applied, the full hydrodynamic solution is obtained through the superposition of these velocity fields.

The equation of sinusoidal motion of the WEC evaluated by SIMO is written as, see MARINTEK (2012b) for details:

$$(M_{WEC} + A_{WEC}(\omega))\ddot{\boldsymbol{x}}_{WEC} + (D_{WEC}(\omega) + D_{PTO})\dot{\boldsymbol{x}}_{WEC} + K_{WEC}\boldsymbol{x}_{WEC} = \boldsymbol{R}_{WEC} \quad (1)$$

where M_{WEC} and D_{PTO} are matrices for the total mass and PTO damping of the WEC, respectively; $A_{WEC}(\omega)$, $D_{WEC}(\omega)$ and K_{WEC} are matrices for the added mass, damping and hydrostatic stiffness evaluated numerically by the hydrodynamic diffraction/radiation software DNV HydroD using the WADAM solver, respectively (DNV, 2013c); ω is the angular frequency of the buoy motion; $\ddot{\boldsymbol{x}}_{WEC}$, $\dot{\boldsymbol{x}}_{WEC}$ and $\boldsymbol{x}_{WEC}$ are the acceleration, velocity and displacement vectors of the WEC, respectively. It should be noted that Eq. (1) is a general formulation of the equation of motion of the WEC. Depending on the simulation procedure, coupled or de-coupled, the excitation force vector $\boldsymbol{R}_{WEC}$ includes effects from the wave, the mooring system, the wind, the current and other forces (MARINTEK, 2012b). The response vectors ($\ddot{\boldsymbol{x}}_{WEC}$, $\dot{\boldsymbol{x}}_{WEC}$ and $\boldsymbol{x}_{WEC}$) in Eq. (1) are only for the WEC that consists of 3-DOF translations and 3-DOF rotations. Section 3.5 discusses the solution methods and the response vectors of the entire WEC system.

Table 3 Geometrical characteristics of the WEC.

Total mass, M_{WEC} [metric tonnes]	100.63
Diameter, d [m]	5
Height, H [m]	10
Draft, T [m]	5
Centre of buoyancy (COB) (x,y,z) [m]	(0, 0, -2.50)
Centre of gravity (COG) (x,y,z) [m]	(0, 0, -2.42)
Damping in six DOFs, D_{PTO} [kNs/m, kNms/rad]	(100, 100, 15, 350, 350, 0)

3.3 Mooring system

A four-line mooring system is used in accordance with Figure 3 above. This mooring configuration is suitable for a FPA WEC, which has strong heave and pitch motions (Fitzgerald and Bergdahl, 2008). The mooring lines are symmetrically attached around the outer rim of the bottom of the WEC. Mooring line 1 is oriented in the positive x-direction, line 2 is oriented in the positive y-direction, and so on; see Figure 3. The initial positions of the lines' fairleads are (2.5, 0, -5) m, (0, 2.5, -5) m, (-2.5, 0, -5) m, and (0, -2.5, -5) m. The lines are anchored in the seabed at a horizontal distance of 74.8 m from the fairleads on the WEC, at a water depth, h, of 50 m. Thus, the entire mooring system is contained within a circle diameter of 154.6 m. The boundary conditions in the anchor point of each mooring line are fixed conditions in all six DOFs at the seabed, whereas the line fairlead attachment to the WEC allows for free rotation. The mooring lines are restricted to have stiffness in the axial direction only, *i.e.* zero bending and torsional stiffness is assumed. The axial force-displacement relation follows a linearly elastic material behaviour. The loading of the mooring lines is characterised by the axial force or, equivalently, the axial stress because the cross section is assumed to be constant along the lines. The geometry, stiffness and mass data are presented in Table 4.

In reality, all structures exhibit some degree of energy loss during movement due to the nonlinearity of the members, energy radiation, and inherent damping (Alipour and Zareian, 2008). In DeepC, the Rayleigh damping formulation is used as structural damping and to incorporate the inherent damping of the mooring lines into the model (DNV, 2012). The damping matrix is proportional to the stiffness matrix and described with parameter D_R, a parameter which is kept constant throughout the analysis to obtain good numerical stability and computational efficiency (DNV, 2010). In MooDy, the damping is included explicitly by a linear visco-elastic material model, using the ratio of critical damping D_C (Palm, 2014). To include the added mass force of the mooring line, a constant added mass coefficient, C_{Mn}, is introduced. In this study, the added mass is assumed to be proportional to the submerged cross section of the mooring line. In addition, the drag coefficients C_{Dt} and C_{Dn} are used to compute the viscous force acting on the longitudinal and transverse directions of mooring line, as discussed by Fitzgerald and Bergdahl (2008).

Table 4 Properties of the mooring lines.

Length, L [m]	100
Diameter, d_m [m]	0.05
Axial stiffness, EA [MN]	100
Mass per unit length, M_m [kg/m]	61
Material density, ρ_{steel} [kg/m^3]	7,800
Normal flow added mass coefficient, C_{Mn} [-]	3.8
Normal flow drag coefficient, C_{Dn} [-]	2.5
Tangential flow drag coefficient, C_{Dt} [-]	0.5
Structural damping coefficient in DeepC, D_R [-]	0.025
Structural critical damping coefficient in MooDy, D_C [-]	0.025

The structural response of the mooring lines is solved through element discretisation with the FE method. In DeepC (DNV, 2012), first-order bar elements are used to represent the mooring lines. All elements are assumed to be straight with a constant cross-sectional area along the element length. The deformation of the model allows for full rotations and translations in three-dimensional spaces.

Each node is restricted to three-DOF translations only. Because each element has two nodes, which are restricted to three DOFs, each element has 2×3 DOFs with only translations. An element of length 1 m has been used in the DeepC mooring simulations. In MooDy, a higher-order FE formulation with discontinuous elements is applied (Palm, 2014). Thus elemental deformation of arbitrary order p is supported, enabling high accuracy with only a few elements for smooth solutions. For any choice of p, each element in MooDy has $(p + 1) \times 3$ DOFs with only translations. In this study, the MooDy simulations were made with a polynomial order $p = 7$ with 10 m long elements. Thus, the main difference between the mooring approximations of MooDy and DeepC for this problem is in the numerical implementation. With respect to all physical parameters such as stiffness and dynamic properties, they are equal (see Table 4).

The first structure response calculations indicated that the stress levels in the mooring lines are typically considerably lower than the design yield stress of the material. Hence, a stress-based approach for fatigue analysis is adopted. The stress history in each mooring line is obtained from the time-domain simulations. Then, the rainflow counting (RFC) method is employed to extract the stress cycles from the stress history and the corresponding stress ranges for the fatigue analysis (Dowling, 2013; Rychlik, 1987). The fatigue damage, FD, is calculated by the Palmgren-Miner cumulative rule using the S-N curve for the material under consideration:

$$FD = \sum_i \frac{n_i S_i^m}{\alpha} \tag{2}$$

In Eq. (2), n_i is the number of axial stress cycles at stress range S_i, which is calculated using the RFC method; and α and m are the material parameters in the S-N diagram, which are set to $10^{12.164}$ and 3 in the current study (DNV, 2010). No fatigue limit is adopted, *i.e.*, all stress ranges contribute to the total fatigue damage. The fatigue damage calculation is carried out using an in-house MATLAB code (MathWorks, 2013).

3.4 Seabed

Seabed conditions vary between different sites depending on *e.g.* the topology and the material property (sand, soil, rock, etc.) of the seabed at the site under consideration. To simplify the analyses in the current study, the seabed is modelled as a horizontal plane considering only a normal force and a tangential force (friction force) induced by the seabed-mooring line contact. The mooring line is assumed to be a rigid body, whereas the seabed is assumed to be elastic with a normal stiffness of 1 MPa and a friction coefficient of 1 (see Palm et al. (2013)). The influence of the friction force of the seabed is evaluated as the friction coefficient times the normal force in the line axis direction. In DeepC, the normal stiffness is modelled as a linear force-displacement relation with no damping (DNV, 2012). In MooDy, a bi-linear spring-damper is used in combination with tangential friction force to describe the seabed model (Palm, 2014). Note that the difference in seabed implementation between the two solvers results in a static force offset; see Section 4.1 for a discussion.

3.5 Solution methods

The equation of motion for the assembled FE model of the WEC system can be written as (see MARINTEK, 2012b):

$$M\ddot{\boldsymbol{x}} + D\dot{\boldsymbol{x}} + K\boldsymbol{x} + \int_0^t h(t-\tau)\dot{\boldsymbol{x}}(\tau)d\tau = \boldsymbol{q}(t, \boldsymbol{x}, \dot{\boldsymbol{x}}) \tag{3}$$

where $\ddot{\boldsymbol{x}}$, $\dot{\boldsymbol{x}}$ and $\boldsymbol{x}$ represent the acceleration, velocity and displacement vectors of the system, respectively; the matrices M, D and K represent the mass of the system (including the ordinary mass and added mass contributions), the damping and the stiffness; and $h(\tau)$ is the retardation function computed by a transform of the frequency-dependent added-mass and damping. The vector $\boldsymbol{q}(t, \boldsymbol{x}, \dot{\boldsymbol{x}})$ represents wave excitation forces, drag force, and any other forces such as wave drift damping. In the coupled simulation procedure, the response vectors ($\ddot{\boldsymbol{x}}$, $\dot{\boldsymbol{x}}$ and $\boldsymbol{x}$) in Eq. (3) consist of six DOFs from the WEC (see Section 3.2) and additional DOFs from the mooring system (see Section 3.3). In the de-coupled simulation procedure, the response vectors ($\ddot{\boldsymbol{x}}$, $\dot{\boldsymbol{x}}$ and $\boldsymbol{x}$) in Eq. (3) consists only of three DOFs representing the DOFs of the mooring system, and the motions of the WEC are included in the right-hand side of the equation as a prescribed external force on the mooring line. The solution to Eq. (3) can be made by convolution integrals; see MARINTEK (2012b) for details.

The dynamic equilibrium of the system is solved with the Newmark-β time stepping scheme. The relationship between the displacement, velocity and acceleration vectors at times t and $t + \Delta t$ are as follows:

$$\dot{\boldsymbol{x}}_{t+\Delta t} = \dot{\boldsymbol{x}}_t + (1-\gamma)\ddot{\boldsymbol{x}}_t \Delta t + \gamma \ddot{\boldsymbol{x}}_{t+\Delta t} \Delta t \tag{4a}$$

$$\boldsymbol{x}_{t+\Delta t} = \boldsymbol{x}_t + \dot{\boldsymbol{x}}_t \Delta t + \left(\frac{1}{2} - \beta\right)\ddot{\boldsymbol{x}}_t (\Delta t)^2 + \beta \ddot{\boldsymbol{x}}_{t+\Delta t} (\Delta t)^2 \tag{4b}$$

where γ and β are parameters that will affect the behaviour of the time stepping, such as accuracy, stability, numerical dispersion and dissipation. In the simulations with DeepC, the parameters are set to $\gamma = 1/2$ and $\beta = 1/4$ (DNV, 2012; MARINTEK, 2012b). These parameter values result in an implicit, unconditionally stable time stepping scheme for linear systems, for which the equilibrium iteration is obtained at every time step (DNV, 2004). MooDy uses the second-order Leap-Frog scheme for time integration, which is a conditionally stable explicit scheme (Press et al., 1990). The stability condition relates the chosen polynomial order and the element size to the maximum time step possible for a stable time integration (Cockburn and Shu, 2001). Further information on the time integration of MooDy is presented in Palm (2014). In this study, the time steps in DeepC and MooDy are $2 \cdot 10^{-3}$ s and $1 \cdot 10^{-5}$ s, respectively. The implicit scheme used in DeepC provides convergence at each time step with numerical diffusion of transients shorter than the time step size, while the explicit scheme in MooDy supports high-frequent fluctuations in the solution with a small numerical diffusion, albeit with a significantly smaller time step.

4 Results

This section presents the results from the simulation procedures T1-T4 shown in Table 1. The first motion analysis for the WEC indicated that there were transient start-up effects in the numerical simulation. After a period of time, the response, predicted by the simulation, reaches harmonic response—the amplitude and period of motion response of the WEC were constant. Therefore, to avoid the transient start-up effects, harmonic results for the interval from 60 s to 120 s were used to compare different simulation procedures. The results are presented according to their order in the simulation process for the mooring system: the static configuration, dynamic motion response, stress response and fatigue damage evaluation.

4.1 Static configuration of the mooring lines

The static configuration is determined by the weight and buoyancy of the WEC and mooring lines. Only the vertical displacement is observed because of the symmetry of mooring system and absence of external horizontal force introduced to the system. In addition, when the WEC is at its static position, approximately 40% of the length of each mooring line is in contact with the seabed (see Figure 4). The results presented in Figure 4 are calculated from the standard numerical setting described in Section 3 using simulation procedure T3.

The position at the fairlead for T2 and T4 are the inputs from T1 and T3, respectively. At the same static position, the corresponding axial force for the mooring line evaluated by MooDy (T2 and T4) is 10% smaller than result evaluated by DeepC (T1 and T3). The main reason for this discrepancy is the difference in the implementation of the seabed model of the two solvers. Nevertheless, irrespective of the choice of simulation procedure and software, minor differences are observed in the predicted axial force for the mooring line; see Table 5 for the static configuration for the fairleads for T1 to T4. In the design process for spread moorings, a static analysis is required to ensure that a sufficient part of their lengths lies on the seabed in order to avoid too large loads on their anchors (Faltinsen, 1990). According to the current results, the coupled and de-coupled simulation procedures show good agreement when used for static analysis of a mooring system.

Many investigations of mooring lines focus on the fairlead point because the axial force is the largest in this location, and it is known that the axial force is lower at the touchdown point (Christiansen et al., 2013; Fitzgerald and Bergdahl, 2008; Johanning et al. 2007; Muliawan et al., 2013; Pascoal et al., 2005; Thies et al., 2014a). The current investigation, with a focus on fatigue, takes a holistic perspective in the comparison of coupled and de-

coupled simulation procedures. Therefore, the fatigue analysis encompasses the four complete mooring lines, and three major points:

- P_0 (fairlead): The attachment point connecting the WEC and mooring line. The most severe fatigue is expected at this location due to the influence from the boundary conditions and constraints.
- P_{30} (mid-point): A point located 30 m (along the mooring line) from its P_0, which is chosen as the middle point between the fairlead and touchdown point.
- P_{60} (touchdown): A point located 60 m (along the mooring line) from its P_0, which is chosen as the critical area of the contact force between the mooring line and seabed.

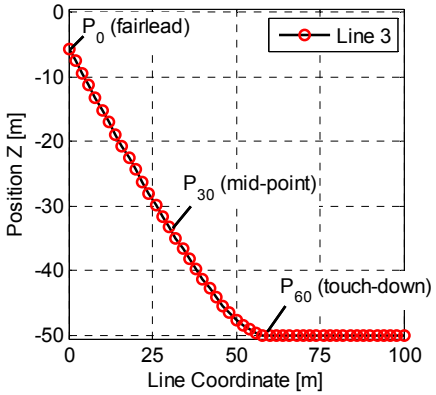

Figure 4 Static configuration for mooring line 3, evaluated by T3.

Table 5 Results of P_0 of mooring line 3 from the static balance analysis.

Types	Position, z [m]	Axial force [N]
T1	-5.63	35427
T2	-5.63	32464
T3	-5.64	35415
T4	-5.64	32453

4.2 Motion response of the mooring lines

Figure 5 shows the harmonic motion response in P_0, P_{30} and P_{60} of mooring line 3 for T1-T4 defined in Table 1. The motion response of the mooring lines is regular and corresponds to the encountered wave period. The largest amplitude of motion occurs close to the mid-point of the mooring lines (P_{30}), whereas the smallest motion response occurs close to the touchdown point, P_{60}; see Figure 5 (b) and (c). The results show relatively good agreement between T1 to T4; only minor differences can be observed.

The motions in the fairlead from T1 and T3 shown in Figure 5 (a) are input data for T2 and T4. By comparing T1 against T2 and T3 against T4, no notable difference is observed from the motion responses evaluated by MooDy and DeepC. According to Figure 5 (c), the MooDy simulations (T2 and T4) are observed to have larger amplitude of motion response. Because the location being evaluated is at the touchdown point close to seabed, the larger-amplitude results are theorised to be due to the different seabed-mooring line contact models; see Section 3.4.

Because the results evaluated by MooDy have the same trend as the results evaluated by DeepC, further comparison is made between T1 and T3 to investigate the influence from de-coupled and coupled simulation procedures, respectively. It is found that the position z of the points evaluated by T3 simulations are lower than those in the T1 simulations. This may due to the weight of the mooring lines which pulls down the WEC; this effect is considered in the coupled model (T3). With respect to the amplitude of the motion response, good agreement is observed at the fairlead (P_0) yet larger discrepancies are observed at P_{30} and P_{60}. At the mid-point of the mooring line (P_{30}), one can observe that the discrepancy in motion response results between T1 and T3 increases from high-position area (crest) to low-position area (trough). We attribute this trend to the seabed friction and restoring force from the mooring line. Both of them dynamically change the mean position of the WEC and consequently the

motion response of the mooring line (see Section 2). However, they can be captured only in the coupled model (T3). At the touchdown point (P_{60}), the de-coupled model (T1) gives the prediction with larger motion amplitude and smaller contact period, due to the fact that the damping effect from the seabed is only implemented by the coupled model (T3).

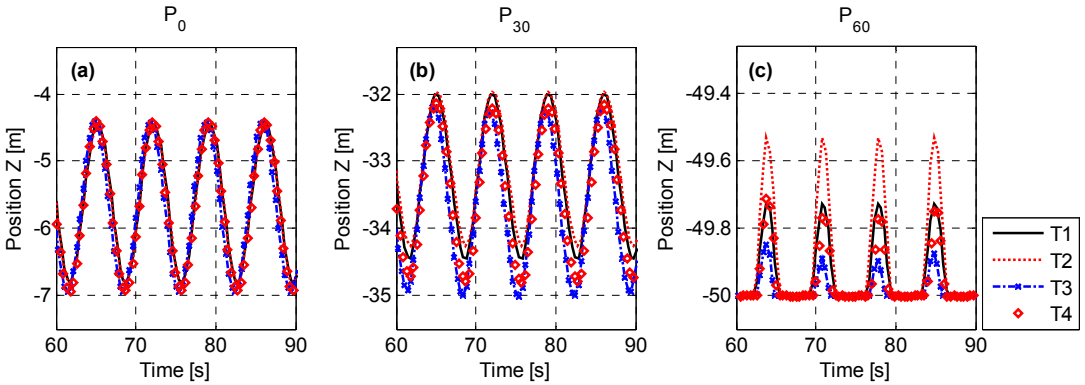

Figure 5 Harmonic motion responses for mooring line 3 at different positions: (a) P_0 (fairlead) (b) P_{30} (mid-point) (c) P_{60} (touchdown).

4.3 Stress response of the mooring lines

The stress response of the mooring line is calculated for the simulation procedures T1-T4 in Table 1; the axial stress is used in the comparison because only the axial stiffness of the mooring line is considered (Section 3.3). Figure 6 shows the stress response in mooring line 3 at P_0, P_{30}, and P_{60}.

Similar to the motion response, the stress response is regular and corresponds to the encountered wave period. In terms of the average of the peak stress values, the largest stress occurs at the fairleads (P_0). A larger distance from the fairleads to the measuring point on the mooring line leads to a smaller average stress value. However, in terms of the amplitude of the stress response, the largest value occurs at the fairleads, and no notable disparity is observed between P_{30} and P_{60}.

The average stress value evaluated by MooDy is slightly smaller than the value evaluated by DeepC. However, the two solvers achieve good agreement with respect to the amplitude of the stress response. It is observed that the stress response evaluated by MooDy resulted in high-frequency ripples. Because these ripples are more obvious at the low-tension area (the trough of the stress response curve) and in the touchdown point (P_{60}), the ripples are likely generated as the mooring lines make contact with the seabed. As the numerical implementation of MooDy has lower diffusion, these ripples are relatively persistent. Moreover, due to the assumption in MooDy that the mooring line is submerged in still water (see Section 3.1), DeepC and MooDy evaluate the relative velocity and acceleration of the mooring lines and water differently. Nevertheless, given a long wave period of 7 s in the present case, the relative motions between the mooring lines and the fluid are comparatively small. As a result, the effects of added mass and drag force on the mooring lines are small and the difference between DeepC and MooDy arising from surrounding fluid motions should therefore be limited.

One can compare T1 and T3 results to investigate differences between the coupled and de-coupled simulation procedures. The prediction for the average stress value is smaller yet the amplitude is larger when using the coupled model (T3). This difference is more notable in the fairlead (P_0) than in the touchdown point (P_{60}). This is because the force from the mooring line to the WEC, included only in the coupled model, instantaneously and directly affects the response at the fairlead points, while the same effect may be mitigated due to the force propagation along the mooring lines. In addition, for three evaluation points (P_0, P_{30}, P_{60}), the

deviation of stress response between T1 and T3 is always smallest at high-tension area (crest) and largest at low-tension area (trough). This result suggests the importance to adopt a coupled model (T3) since it accounts for seabed-mooring contact. The influence on the fatigue damage from the stress amplitude is presented in Section 4.4.

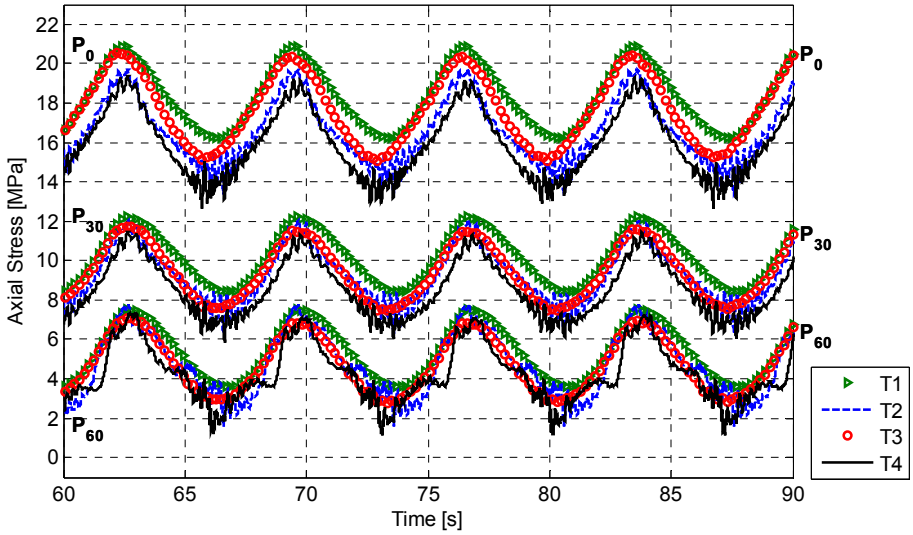

Figure 6 Harmonic axial stress responses of mooring line 3 in P_0, P_{30} and $P6_0$, where T1-T4 are represented by green triangles, a blue dash line, red circles, and a black solid line, respectively.

4.4 Fatigue damage evaluation of the mooring lines

Figure 7 presents the results from the fatigue damage analysis for each simulation procedure T1-T4 lasting one minute. The results show that the fatigue damage is the largest at the fairlead (P_0) of the mooring line. The accumulated fatigue damage decreases as the distance from the fairleads increases. However, the fatigue damage increases in the touchdown region (around P_{60}). Among the mooring lines, mooring lines 2 and 4 have the same accumulated damage for their location at the beam sea. The largest fatigue damage occurs when the mooring line is positioned to head into the encounter wave (only mooring line 3 in this study). However, mooring line 1 shows different trends between the simulation procedures; these trends need to be investigated in future work.

There are two differences between MooDy and DeepC which influence the outcome of the fatigue assessment. Firstly, the fatigue damage evaluated by MooDy (T2 and T4) is generally larger than the fatigue damage evaluated by DeepC (T1 and T3). The larger fatigue damage is attributed to the high-frequency ripples shown in the MooDy results (see Figure 6). Such ripples last longer in a high-order FE formulation, and therefore the number of stress cycles increases dramatically and yields a significant increase in the fatigue damage evaluation. Secondly, both solvers exhibit some degree of influence from the seabed contact. However, stress results calculated by MooDy are more sensitive to the seabed contact; the fatigue damage around the touchdown point (P_{60}) is significantly diverse. It should be noted that the sudden contact force, induced by the seabed-mooring line contact, might cause numerical oscillations in the high-order numerical scheme which would exaggerate the influence of the seabed on the fatigue estimation.

Comparing cases T1 and T3 clearly shows the differences between the coupled and de-coupled simulation procedures. The results from the two procedures exhibit relatively good agreement in terms of the trend of the fatigue damage accumulation along the mooring lines. Based on the current fatigue model, the fatigue damage is exclusively determined by the

amplitude of stress response (see Section 3.3). As a result, it is reasonable to get larger fatigue damage in the coupled model (T3) due to the larger stress amplitude shown in Figure 6.

On the one hand, the de-coupled model simplifies the system complexity to benefit the numerical stability. On the other hand, the use of de-coupled model may lead to under-prediction of the fatigue damage of the mooring lines (based on the comparison of T1 and T3 results). In addition, since the cost of moorings is approximately 30% of the budget of a WEC system, and that failure of moorings in positioning can lead to failure of the entire WEC system (Martinelli et al., 2012), it is vital to have reliable prediction tools in the early design. This investigation shows that since there is no evident gain from using the de-coupled simulation procedure, the coupled simulation procedure is recommended given its accuracy in the fatigue damage evaluation. Note, however, future work is needed to investigate if this simulation procedure is recommended also for modelling and analysis of larger arrays of WECs.

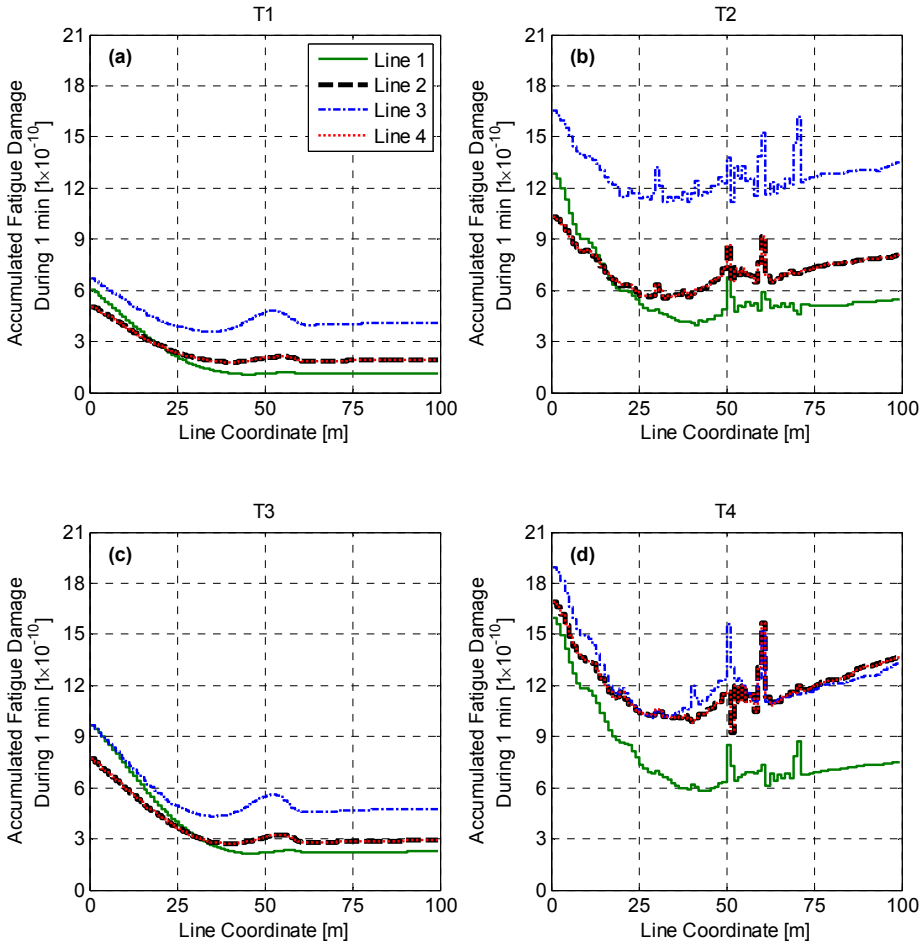

Figure 7 Presentation of the results from the fatigue damage calculations for the four types of simulation procedures along the whole mooring line from the fairlead to the anchor point (line coordinate from 0 to 100 m). Mooring lines 1-4 are represented by a green thin line, a black dash line, a blue dash-dotted line and a red dotted line, respectively.

5 Response analysis and discussion

Some of the numerical and physical parameters have a considerable influence on the results from the simulations and in particular the fatigue damage analyses. With regards to numerical parameters, the influence of the mesh size of the mooring lines and the structural damping of the mooring lines are presented in Sections 5.1-5.2. Furthermore, the influences of three physical parameters, including the period and height of the encountered waves, length of mooring lines, bending and torsional stiffness of mooring lines, are investigated and discussed

in Sections 5.3-5.5. The influence of other parameters, such as wave drift force, specified force, and artificial stiffness, is presented in Yang et al. (2014).

Table 6 summarises all cases investigated in the systematic fatigue response analysis. It was carried out by the T3 simulation procedure (see Table 1) because it captured the necessary coupling effect with reasonable computational effort. The standard numerical setting is presented in Table 7, in which only one quantity setting is varied at a time using the values presented in Table 6. Cases E7, RD3, W6, L1 and B1 are all standard cases. Figure 8 shows the accumulated fatigue damage in P_0 of mooring line 3 over the period of one minute for all cases; all of the standard cases are shown in red bars.

Table 6 Cases in the systematic fatigue response analysis.

Variable	Case	Description
Mesh size of the mooring line [m]	E1	10.00
	E2	7.50
	E3	5.00
	E4	4.00
	E5	3.00
	E6	2.00
	E7	1.00
	E8	0.50
	E9	0.25
Structural damping of the mooring line [-]	RD1	0.001
	RD2	0.010
	RD3	0.025
Encountered wave (height [m] / period [s])	W1	1 / 3
	W2	1 / 5
	W3	1 / 7
	W4	2 / 3
	W5	2 / 5
	W6	2 / 7
	W7	4 / 3
	W8	4 / 5
	W9	4 / 7
Length of the mooring line [m]	L1	100
	L2	95
	L3	90
Bending and torsion stiffness of the mooring line [Nm^2 / Nm^2/rad]	B1	0 / 0
	B2	94300 / 8500

Table 7 Standard numerical setting for the systematic fatigue response analysis.

Variable	Description
Mesh size of the mooring line [m]	1.00
Structural damping of the mooring line in DeepC [-]	0.025
Encountered wave (height [m] / period [s])	2 / 7
Length of the mooring line [m]	100
Bending and torsional stiffness of the mooring line [Nm^2 / Nm^2/rad]	0 / 0

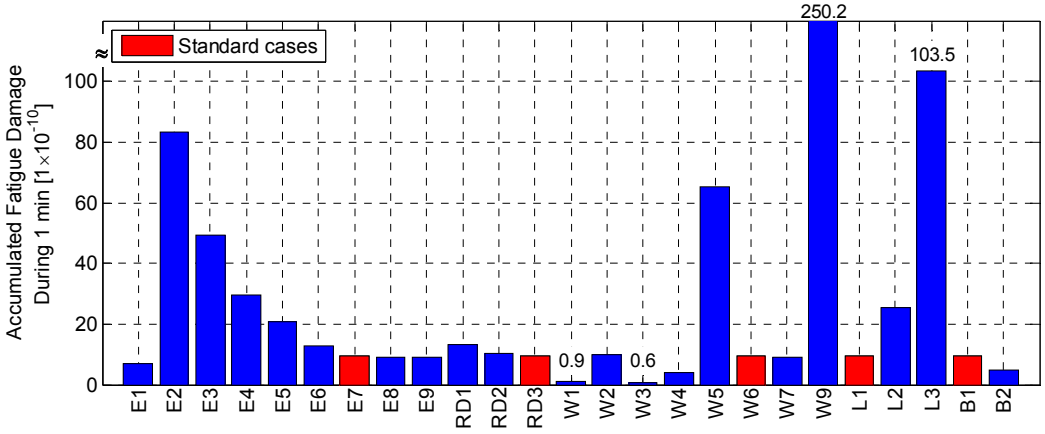

Figure 8 Summary of the results from the accumulated fatigue damage in P_0 of mooring line 3; see Table 6 for a definition of the numerical simulation cases.

5.1 Convergence of the mesh size

A smaller element size generally yields more accurate results in a FE analysis. However, the smaller mesh requires larger computational effort and time. Thus, a balance between the accuracy of the analysis and reasonable computational effort must be achieved. However, because of the various size scales of the numerical model, there is no consistent agreement on what mesh size that should be used to obtain satisfactory converging results for fatigue damage. Hence, a mesh convergence analysis is carried out in which the element length of the mooring lines is varied according to E1 to E9 in Table 6.

The finite elements in each mooring line have the same size (*i.e.,* the element size is uniformly distributed). The variation in the results with respect to element size is shown in Figure 8 by bars E1-E9. The element convergence analysis shows that the calculation of the fatigue damage is relatively insensitive to an element size of less than 1 m. Thus, the 1 m element size is selected as the standard for this study.

5.2 Structural damping of the mooring line

As noted in Section 3.3, all structures show some degree of energy loss during motion, which is referred to as the three main sources in the numerical analysis: the nonlinearity of the members, the energy radiation, and the inherent damping (Alipour and Zareian, 2008). A constant damping is often applied for better numerical stability. However, in reality, the damping can vary significantly, and constant damping can result in an unreasonable response in the time history analysis (Kandge, 2007; Spears and Jensen, 2012). Therefore, three values of the Rayleigh damping are chosen, in which RD3 is the recommended value from DNV (2012).

Figure 9 shows that although the average and amplitude of stress are not affected by the structural damping, the oscillations of the stress response are significantly reduced when the value of the structural damping is increased (RD1<RD2<RD3). These oscillations result in the larger fatigue damage of the mooring line, as shown by bars RD1-RD3 in Figure 8. This observation also explains why MooDy predicted larger fatigue damage in the mooring lines

due to the high-frequency ripples shown in the stress response; see Sections 4.3 and 4.4. Because MooDy uses a different implementation of the damping model, further investigation is needed to find a suitable value describing the structural damping of mooring lines.

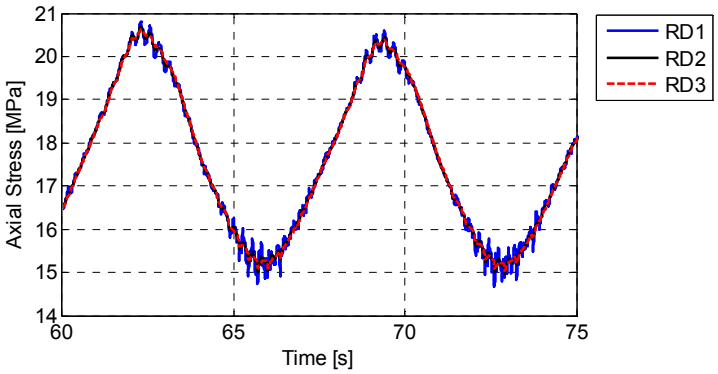

Figure 9 Axial stress responses in P_0 of mooring line 3 for different structural dampings.

5.3 Encountered wave height and period

Because the encountered wave is a random condition, it is important to understand the response of the WEC corresponding to different wave conditions. As a result, three wave heights and three wave periods were studied according to the combinations summarised in Table 6. As noted in Section 3.1, the resonant period of the WEC is close to 5 s.

The results from the variation of the wave height and wave period are shown in Figure 8; see bars W1-W9 with the encountered wave information, as shown in Table 6. W8 is excluded from this study because the simulation did not converge. An influence on the fatigue damage is observed in the remaining cases. A higher wave height (larger energy extraction) induces larger fatigue damage; therefore, a WEC designer must strike a cost balance between the energy extractions, the structural life of the WEC, and safety parameters involved. By using the coupled model, one can observe significant nonlinear physical interaction between the WEC, mooring lines, and environment, *i.e.*, a change in wave conditions leads to exaggerated change in fatigue life of mooring lines. Thus, the usage of a linear response model by the de-coupled model is questionable. Nevertheless, the current results show that the fatigue damage is significantly affected by the encountered wave in terms of both the wave period and wave height. Designing a mooring system suitable for a larger range of wave conditions is an important topic for future study.

5.4 Length of the mooring line

The length of the mooring line, together with the position of the anchor points, determines the static configuration of the mooring system. Mooring line length is an important design parameter that influences the main characteristic of a mooring system. In general, a shorter mooring line limits the movement of the WEC unit, but the increased pretension, *i.e.,* the axial stress of the mooring line at still water conditions, reduces the slack situation if the system is faced with severe wave conditions. It is of interest to investigate whether the length of the mooring line will also affect its fatigue damage. The shortest length of a mooring line in this research is 90 m because this is the shortest length which would not cause any line tension force acting on the anchor point.

Figure 10 (a) shows the stress response in P_0 of mooring line 3. The shorter mooring line pulls down the WEC unit more (L3<L2<L1). As a result, the average position of the fairlead (P_0) is the lowest in case L3. Because the mooring line length investigated in this study is still longer than the absolute distance between the fairlead and anchor point, the motion of the WEC is not significantly influenced, this is verified by the fact that the amplitudes of the

motion response are similar in the three cases. However, when the mooring line length is 10% shorter, the greater average stress triples and the stress amplitude doubles in size. Figure 10 (b) illustrates that these stresses also resulted in a ten-fold increase in fatigue damage (bars L1-L3 in Figure 8). This investigation confirms that the current design length of the mooring line (L1) is a suitable configuration with respect to its fatigue life.

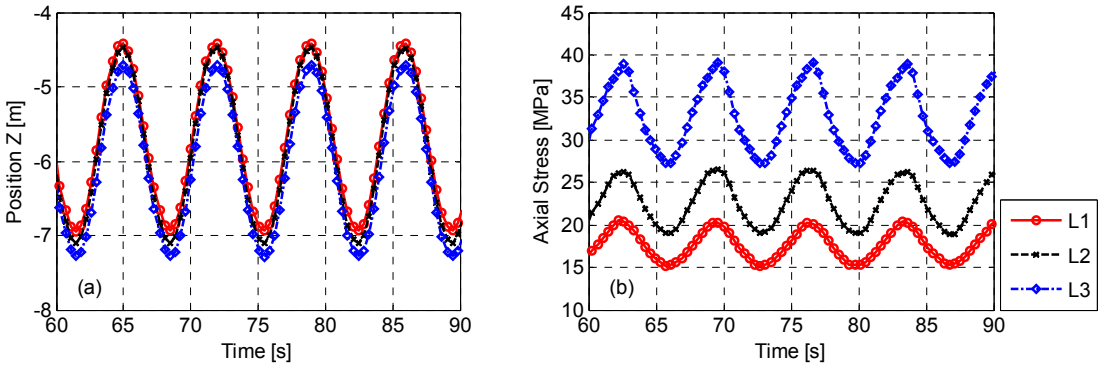

Figure 10 (a) Motion and (b) stress responses in P_0 of mooring line 3 for different lengths of the mooring line.

5.5 Bending and torsional stiffness of the mooring line

In the simulations presented in the former sections, an assumption was made according to Fitzgerald and Bergdahl (2008) that for the current design, the bending and torsional stresses of mooring lines can be neglected. However, in case a different mooring system is used, the bending and torsional stiffness of the mooring lines may need to be considered (DNV, 2010). Therefore, a flexible pipe designed by Furukawa Electric Co. (Chiyoda Corporation, 2011) is selected for comparison due to its bending and torsional stiffness properties.

As shown in Figure 11 (a), the motion response is not affected and no horizontal motion is observed because the regular wave condition is applied to a symmetrical WEC system. However, there is a significant decrease in the average axial stress and stress amplitude in mooring line (Figure 11 (b)), leading to a 40% decrease in fatigue damage shown in Figure 8; see Bars B1-B2 with mooring line properties, as shown in Table 6. The fatigue damage contribution from the bending and torsion stresses should be investigated in future research.

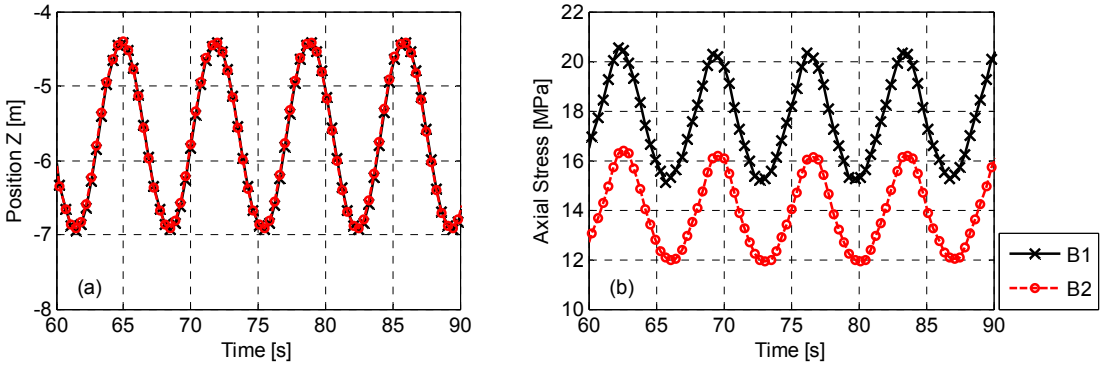

Figure 11 (a) Motion and (b) stress responses in P_0 of mooring line 3 for different mooring line properties.

6 Fatigue damage analysis for irregular wave conditions

A fatigue analysis using regular wave conditions for one minute was made to compare different simulation procedures. In practice, however, a long-term irregular wave analysis is

required to perform an adequate fatigue analysis. Thus, it is important to test whether the proposed simulation procedures are feasible with respect to the computational time for a fatigue analysis in a long-term irregular wave condition.

For this purpose, one irregular wave case was tested. This case was simulated with a JONSWAP wave spectrum using a significant wave height of 3.2 m, a peak period of 7.9 s, and a peakedness factor of 3.0, representative of a 1-year condition at Chinese Bohai Bay; see Cheng et al. (2014) for details. This location data was chosen because it is suitable for the operational conditions of the current WEC. The irregular wave case was carried out by simulation procedures T1 and T3, as shown in Table 1, and with all other modelling parameters identical to those presented in Section 3. The simulation length lasted three hours, a sufficient amount of time to provide adequate statistics for the fatigue damage analysis (DNV, 2010). Figure 12 shows the motion and stress response in P_0 of mooring line 3 during the time period from 60 to 360 s. The corresponding largest accumulated fatigue damage for 3 hours occurs in P_0 of mooring line 1 for the values $1.4 \cdot 10^{-5}$ (T1) and $8.5 \cdot 10^{-6}$ (T3), equivalent to fatigue lives of 24.7 and 40.1 years, respectively. In contrast to the fatigue damage results for the regular wave case presented in Section 4.4., the de-coupled simulation procedure predicts a longer fatigue life. However, an analysis of the vertical WEC motion, for the irregular wave case using the de-coupled model, showed that it was larger compared to the coupled model, see Figure 12 (a). It was also observed during post-processing that for the largest wave heights, the WEC had unrealistically large vertical motion. The explanation seems to be due to the absence of restoring forces from the mooring lines in the de-coupled simulation procedure. This behaviour was not observed in the simulated regular wave cases. To conclude, the coupled simulation procedure is recommended. As a final remark, a comparison of the CPU time needed for the de-coupled and coupled simulation procedures, respectively, showed no significant differences, when the simulation is carried out using a computer with a CPU Intel Core i7-3770 @ 3.40 GHz.

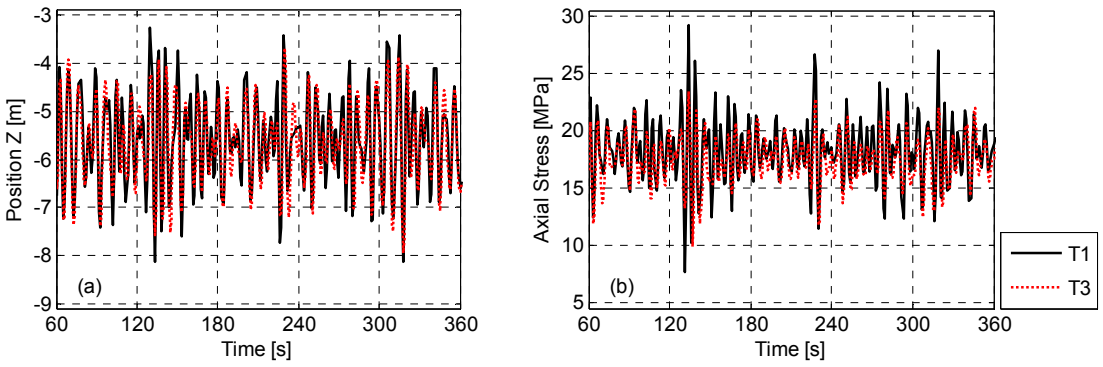

Figure 12 (a) Motion and (b) stress responses in P_0 of mooring line 3 in an irregular wave condition.

7 Conclusions

The investigation contributes to the fatigue design of mooring lines used for WECs. Few investigations have been reported in the public literature on this topic, especially where coupled and de-coupled simulation procedures are compared with regard to the fatigue life prediction of mooring lines. Hence, this study compares four types of simulation procedures for simulating the hydrodynamic and structural response of a WEC and its mooring lines with respect to the reliability of the prediction of fatigue damage. The following summarises the observations and recommendations made by the authors concerning how to complete a fatigue analysis of mooring line systems for the WECs using MooDy, DeepC and the proposed simulation procedures.

As shown in Sections 4 and 6, the coupled and de-coupled simulation procedures generate different fatigue results for the studied cases under moderate wave conditions. Some of the reasons are due to the limitations in the de-coupled simulation procedure, such as the lack of dynamic influence from mooring, linearity assumption and absence of wave drift force. These differences are expected to be larger during more severe wave conditions. From a fatigue design perspective, since the CPU time are about the same for the two simulation procedures, the coupled simulation procedure is considered as the better option for comprehensive studies of WEC systems.

Different numerical implementations of the cable dynamics employed by DeepC and MooDy have significant impact on the fatigue assessment of the mooring lines. DeepC is integrated commercial software, and its numerical robustness is sound for the investigation of WEC systems. In the current study case, it is shown that the coupling effect available in DeepC is crucial for the fatigue damage analysis of the mooring line. Consequently, the coupled approach in DeepC is recommended to be used. It is also recommended for the mooring systems of which the contribution from bending and torsional stress cannot be neglected. However, because of the small wave amplitude theory employed by DeepC, the usage of DeepC on critical wave conditions should be examined for each individual WEC system.

The results from MooDy and DeepC reached good agreement with respect to the average values and the amplitudes of the motion and stress responses. However, the fatigue damage evaluated by MooDy was generally larger than the fatigue damage evaluated by DeepC. This difference is attributed to the high-frequency ripples shown in the MooDy results (see Section 4.3 and 4.3). More detailed studies on the source of these ripples are needed, in order to quantify the extent of different contributions, namely the numerical artefact from FE formulation and physical contact between mooring lines and seabed.

Some design parameters, *i.e.,* the length and structural characteristics of the mooring lines, are found to have a considerable influence on the structural behaviour of a mooring system and its fatigue life. These influences indicate that it is important to consider the fatigue life assessment at an early stage during the design phase of a new WEC mooring system, preferably using a coupled simulation procedure.

Acknowledgements

The authors gratefully acknowledge the financial support from the Swedish Energy Agency for the project “Durability analysis of cables and mooring used in systems for harvesting of renewable ocean energy”, Contract No. 36357-1.

References

Abouelfadl, W., Gowthaman, P., Joe-Joe, C., Fraser, C., 2013. Cost effective method for shallow water cable laying, Proceeding of the ASME 32nd International Conference on Ocean, Offshore and Arctic Engineering (OMAE 2013). American Society of Mechanical Engineers, Nantes, France.

Alipour, A., Zareian, F., 2008. Study Rayleigh damping in structures; uncertainties and treatments, 14th world conference on earthquake engineering, Beijing, China.

Ambühl, S., Kramer, M., Sørensen, J.D., 2015. Different reliability assessment approaches for wave energy converters, Proceeding of the 11th European Wave and Tidal Energy Conference (EWTEC 2015), Nantes, Frances.

Babarit, A., 2013. On the park effect in arrays of oscillating wave energy converters. Renewable Energy 58, 68-78.

Babarit, A., Hals, J., Muliawan, M.J., Kurniawan, A., Moan, T., Krokstad, J., 2012. Numerical benchmarking study of a selection of wave energy converters. Renewable Energy 41 (0), 44-63.

Barstow, S., Mørk, G., Mollison, D., Cruz, J., 2008. The wave energy resource, Ocean wave energy. Springer-Verlag, Heidelberg, Berlin, Germany, pp. 93-132.

Berteaux, H.O., 1976. Oceanographic buoy systems, classes, designs, and components-Buoy system design, in: McCormick, M.E. (Ed.), Buoy engineering. Wiley-Interscience, New York, USA.

Bhinder, M.A., Karimirad, M., Weller, S., Debruyne, Y., Guérinel, M., Sheng, W., 2015. Modelling mooring line non-linearities (material and geometric effects) for a wave energy converter using AQWA, SIMA and Orcaflex, Proceeding of the 11th European Wave and Tidal Energy Conference (EWTEC 2015), Nantes, Frances.

Budar, K., Falnes, J., 1975. A resonant point absorber of ocean-wave power. Nature 256 (5517), 478-479.
Carbon Trust, 2011. Marine renewables green growth paper.
Cerveira, F., Fonseca, N., Pascoal, R., 2013. Mooring system influence on the efficiency of wave energy converters. International Journal of Marine Energy 3–4 (0), 65-81.
Cheng, Z., Yang, J., Hu, Z., Xiao, L., 2014. Frequency/time domain modeling of a direct drive point absorber wave energy converter. Science China Physics, Mechanics and Astronomy 57 (2), 311-320.
Chiyoda Corporation, 2011. Preliminary feasibility study on CO2 carrier for ship-based CCS. Global Carbon Capture and Storage Institute Ltd (GCCSI).
Christiansen, N.H., Voie, P.E.T., Høgsberg, J., Sødahl, N., 2013. Efficient mooring line fatigue analysis using a hybrid method time domain simulation scheme, Proceeding of the ASME 32nd International Conference on Ocean, Offshore and Arctic Engineering (OMAE 2013). American Society of Mechanical Engineers, Nantes, France.
Cockburn, B., Shu, C.-W., 2001. Runge–Kutta discontinuous Galerkin methods for convection-dominated problems. Journal of Scientific Computing 16 (3), 173-261.
Davies, P., 2009. Guidelines for design basis of marine energy conversion systems. The Charlesworth Group, European Marine Energy Centre Ltd (EMEC), Wakefield, UK.
DNV, 2004. DeepC – deep water coupled analysis tool. A white paper Rev 3. Det norske Veritas (DNV), Høvik, Norway.
DNV, 2005. Guidelines on design and operation of wave energy converters. Carbon Trust and Det norske Veritas (DNV).
DNV, 2010. Offshore standard DNV-OS-E301 Position mooring. Det norske Veritas (DNV).
DNV, 2012. RIFLEX theory manual Version 4.0. Det norske Veritas (DNV), Høvik, Norway.
DNV, 2013a. Sesam DeepC, V4.7-07 ed. Det norske Veritas (DNV), Høvik, Norway.
DNV, 2013b. RIFLEX user manual Version 4.0 Rev 3. Det norske Veritas (DNV) Høvik, Norway.
DNV, 2013c. Sesam HydroD, V4.7-07 ed. Det norske Veritas (DNV), Høvik, Norway.
Dowling, N.E., 2013. Fatigue of materials: Introduction and stress-based approach, in: Stark, H. (Ed.), Mechanical behavior of materials: Engineering methods for deformation, fracture, and fatigue, 4 ed. Angshuman Chakraborty, Westford, USA.
Falcão, A.F.d.O., 2010. Wave energy utilization: a review of the technologies. Renewable and Sustainable Energy Reviews 14 (3), 899-918.
Faltinsen, O.M., 1990. Stationkeeping, in: Dyer, I., Taylor, R.E., Newman, J.N., Price, W.G. (Eds.), Sea loads on ships and offshore structures. Cambridge University Press, Cambridge, UK, pp. 257-281.
Fitzgerald, J., 2009. Position mooring of wave energy converters–An engineering study into the mooring of structures in a highly exposed shallow ocean regime, within the context of the economics of renewable energy conversion, Department of Civil and Environmental Engineering. Chalmers University of Technology, Göteborg, Sweden.
Fitzgerald, J., Bergdahl, L., 2008. Including moorings in the assessment of a generic offshore wave energy converter: A frequency domain approach. Marine Structures 21 (1), 23-46.
Gao, Z., Bingham, H.B., Nicholls-Lee, R., Adam, F., Karmakar, D., Karr, D.G., Catipovic, I., Colicchio, G., Sheng, W., Liu, P., Takaoka, Y., Slätte, J., Shin, H.-K., Mavrakos, S.A., Jhan, Y.-T., Ren, H., 2015. Offshore renewable energy, 19th International Ship and Offshore Structures Congress. ISSC Committee V.4, Cascais, Portugal.
Harnois, V., Weller, S.D., Johanning, L., Thies, P.R., Le Boulluec, M., Le Roux, D., Soulé, V., Ohana, J., 2015. Numerical model validation for mooring systems: Method and application for wave energy converters. Renewable Energy 75 (0), 869-887.
Jacobson, P., 2011. Mapping and assessment of the United States ocean wave energy resource. Electric Power Research Institute, Palo Alto, California, USA.
Johanning, L., Smith, G.H., Wolfram, J., 2006. Mooring design approach for wave energy converters. Proceedings of the Institution of Mechanical Engineers Part M: Journal of Engineering for the Maritime Environment 220 (4), 159-174.
Johanning, L., Smith, G.H., Wolfram, J., 2007. Measurements of static and dynamic mooring line damping and their importance for floating WEC devices. Ocean Engineering 34 (14–15), 1918-1934.
Kandge, G.M., 2007. Influence of mode dependent Rayleigh damping on transient stress response, Department of Mechanical Engineering. Blekinge Institute of Technology, Karlskrona, Sweden.
Liu, Y., Bergdahl, L., 1997. Frequency-domain dynamic analysis of cables. Engineering Structures 19 (6), 499-506.
López-Pavón, C., Watai, R.A., Ruggeri, F., Simos, A.N., Souto-Iglesias, A., 2013. Influence of wave induced second-order forces in semi-submersible FOWT mooring design, Proceeding of the ASME 32nd International Conference on Ocean, Offshore and Arctic Engineering (OMAE 2013). American Society of Mechanical Engineers, Nantes, France.
Magagna, D., MacGillivray, A., Jeffrey, H., Hanmer, C., Raventos, A., Badcock-Broe, A., Tzimas, E., 2014. Wave and tidal energy strategic technology agenda, 2 ed. published by SI Ocean.
MARINTEK, 2012a. SIMO – general description Version 4.0. Norwegian Marine Technology Research Institute (MARINTEK), Trondheim, Norway.
MARINTEK, 2012b. SIMO – theory manual Version 4.0 Rev 1. Norwegian Marine Technology Research Institute (MARINTEK), Trondheim, Norway.
Martinelli, L., Ruol, P., Cortellazzo, G., 2012. On mooring design of wave energy converters: The Seabreath application, in: Lynett, P., Smith, J.M. (Eds.), Proceeding of the International Conference on Coastal Engineering (ICCE 2012)-Coastal Engineering Proceedings, Santander, Spain, p. 3.
MathWorks, 2013. MATLAB, R2013b ed. The MathWorks Inc., Natick, MA, USA.
Muliawan, M.J., Gao, Z., Moan, T., Babarit, A., 2013. Analysis of a two-body floating wave energy converter with particular focus on the effects of power take-off and mooring systems on energy capture. Journal of Offshore Mechanics and Arctic Engineering 135 (3), 1-12.
Murphy, S., Bhinder, M.A., Casaubieilh, P., Sheng, W., 2015. Effects of tidal range on mooring systems of wave energy converters, Proceeding of the 11th European Wave and Tidal Energy Conference (EWTEC 2015), Nantes, Frances.

NREL, SNL, 2014. WEC-Sim. National Renewable Energy Laboratory (NREL) and Sandia National Laboratories (SNL), USA.
Palm, J., 2014. Developing computational methods for moored floating wave energy devices, Department of shipping and marine technology. Chalmers university of technology, Göteborg, Sweden.
Palm, J., Eskilsson, C., Moura Paredes, G., Bergdahl, L., 2013. CFD simulation of a moored floating wave energy converter, Proceeding of the 10th European Wave and Tidal Energy Conference (EWTEC 2013). European Wave and Tidal Energy Conference, Aalborg, Denmark.
Paredes, G.M., Palm, J., Eskilsson, C., Bergdahl, L., Taveira-Pinto, F., 2015. Experimental investigation of mooring configurations for wave energy converters, Proceeding of the 11th European Wave and Tidal Energy Conference (EWTEC 2015), Nantes, Frances.
Pascoal, R., Huang, S., Barltrop, N., Guedes Soares, C., 2005. Equivalent force model for the effect of mooring systems on the horizontal motions. Applied Ocean Research 27 (3), 165-172.
Press, W.H., Flannery, B.P., Teukolsky, S.A., Vetterling, W.T., 1990. Numerical recipes. Cambridge University Press Cambridge, New York, USA.
Ridge, I.M.L., Banfield, S.J., Mackay, J., 2010. Nylon fibre rope moorings for wave energy converters, OCEANS 2010 Conference, Seattle, Washington, USA, pp. 1-10.
Rychlik, I., 1987. A new definition of the rainflow cycle counting method. International Journal of Fatigue 9 (2), 119-121.
Siddorn, P., Taylor, R.E., 2008. Diffraction and independent radiation by an array of floating cylinders. Ocean Engineering 35 (13), 1289-1303.
Soulard, T., Babarit, A., Borgarino, B., Wyns, M., Harismendy, M., 2013. C-HYP: a combined wave and wind energy platform with balanced contributions, Proceeding of the ASME 32nd International Conference on Ocean, Offshore and Arctic Engineering (OMAE 2013). American Society of Mechanical Engineers, Nantes, France.
Spears, R.E., Jensen, S.R., 2012. Approach for selection of Rayleigh damping parameters used for time history analysis. Journal of Pressure Vessel Technology 134 (6), 1-7.
STA, 2014. OrcaFlex. Stewart Technology Associates (STA), Houston, TX, USA.
Thies, P.R., Johanning, L., Harnois, V., Smith, H.C.M., Parish, D.N., 2014a. Mooring line fatigue damage evaluation for floating marine energy converters: Field measurements and prediction. Renewable Energy 63 (0), 133-144.
Thies, P.R., Johanning, L., McEvoy, P., 2014b. A novel mooring tether for peak load mitigation: Initial performance and service simulation testing. International Journal of Marine Energy 7 (0), 43-56.
Thies, P.R., Johanning, L., Smith, G.H., 2011a. Towards component reliability testing for marine energy converters. Ocean Engineering 38 (2–3), 360-370.
Thies, P.R., Johanning, L., Smith, G.H., 2011b. Assessing mechanical loading regimes and fatigue life of marine power cables in marine energy applications. Proceedings of the Institution of Mechanical Engineers, Part O: Journal of Risk and Reliability.
Thies, P.R., Johanning, L., Smith, G.H., 2012. Lifecycle fatigue load spectrum estimation for mooring lines of a floating marine energy converter, Proceeding of the ASME 31st International Conference on Ocean, Offshore and Arctic Engineering (OMAE 2012). American Society of Mechanical Engineers, Rio de Janeiro, Brazil, pp. 667-676.
Thomsen, J.B., Ferri, F., Kofoed, J.P., 2015. Assessment of current state of mooring design in the Danish wave energy sector, Proceeding of the 11th European Wave and Tidal Energy Conference (EWTEC 2015), Nantes, Frances.
Vicente, P.C., Falcão, A.d.O., Gato, L.M.C., Justino, P.A.P., 2009a. Hydrodynamics of triangular-grid arrays of floating point-absorber wave energy converters with inter-body and bottom slack-mooring connections, Proceedings of the 8th European Wave and Tidal Energy Conference (EWTEC 2009), Uppsala, Sweden.
Vicente, P.C., Falcão, A.d.O., Gato, L.M.C., Justino, P.A.P., 2009b. Dynamics of arrays of floating point-absorber wave energy converters with inter-body and bottom slack-mooring connections. Applied Ocean Research 31 (4), 267-281.
Vicente, P.C., Falcão, A.F.O., Justino, P.A.P., 2011a. Non-linear slack-mooring modelling of a floating two-body wave energy converter, Proceedings of the 9th European Wave and Tidal Energy Conference (EWTEC 2011), Southampton, UK.
Vicente, P.C., Falcão, A.F.O., Justino, P.A.P., 2011b. Optimization of mooring configuration parameters of floating wave energy converters, Proceedings of the ASME 30th International Conference on Ocean, Offshore and Arctic Engineering, Vol 5: Ocean Space Utilization ; Ocean Renewable Energy (OMAE2011). American Society of Mechanical Engineers, New York, pp. 759-765.
Yang, S.-H., Ringsberg, J.W., Johnson, E., 2014. Analysis of mooring lines for wave energy converters - A comparison of de-coupled and coupled simulation procedures, Proceeding of ASME 33rd International Conference on Ocean, Offshore and Arctic Engineering (OMAE 2014). American Society of Mechanical Engineers San Francisco, California.

Figure captions

Figure 1 Schematic layout of a WEC system and its components; see Section 3 for details.
Figure 2 Workflow of the simulation procedures used in the current study.
Figure 3 Illustration of the set-up of the WEC system comprised of the WEC, the four mooring lines, the water with waves, and the seabed. A Cartesian coordinate system, *xyz*, defines the orientation of the illustration, where the origin is located at the water surface at the WEC equilibrium position.
Figure 4 Static configuration for mooring line 3, evaluated by T3.
Figure 5 Harmonic motion responses for mooring line 3 at different positions: (a) P_0 (fairlead) (b) P_{30} (mid-point) (c) P_{60} (touchdown).
Figure 6 Harmonic axial stress responses of mooring line 3 in P_0, P_{30} and $P6_0$, where T1-T4 are represented by green triangles, a blue dash line, red circles, and a black solid line, respectively.
Figure 7 Presentation of the results from the fatigue damage calculations for the four types of simulation procedures along the whole mooring line from the fairlead to the anchor point (line coordinate from 0 to 100 m). Mooring lines 1-4 are represented by a green thin line, a black dash line, a blue dash-dotted line and a red dotted line, respectively.
Figure 8 Summary of the results from the accumulated fatigue damage in P_0 of mooring line 3; see Table 6 for a definition of the numerical simulation cases.
Figure 9 Axial stress responses in P_0 of mooring line 3 for different structural dampings.
Figure 10 (a) Motion and (b) stress responses in P_0 of mooring line 3 for different lengths of the mooring line.
Figure 11 (a) Motion and (b) stress responses in P_0 of mooring line 3 for different mooring line properties.
Figure 12 (a) Motion and (b) stress responses in P_0 of mooring line 3 in an irregular wave condition.

Table captions

Table 1 Presentation of the four types of simulation procedures that are compared in the current investigation.
Table 2 Environmental conditions in the case study.
Table 3 Geometrical characteristics of the WEC.
Table 4 Properties of the mooring lines.
Table 5 Results of P_0 of mooring line 3 from the static balance analysis.
Table 6 Cases in the systematic fatigue response analysis.
Table 7 Standard numerical setting for the systematic fatigue response analysis.